Available online at www.sciencedirect.com
SCIENCE DIRECT®
Journal of Solid State Chemistry 177 (2004) 2740–2748
JOURNAL OF SOLID STATE CHEMISTRY
http://elsevier.com/locate/jssc

Subsolidus phase relations and crystal structures of the mixed-oxide phases in the In_2O_3–WO_3 system

Annette P. Richard and Doreen D. Edwards*

Materials Science and Engineering, School of Engineering, Alfred University, 2 Pine Street, Alfred, NY 14802, USA

Received 6 January 2004; received in revised form 31 March 2004; accepted 4 April 2004

Abstract

Subsolidus phase relationships in the In_2O_3–WO_3 system at 800–1400°C were investigated using X-ray diffraction. Two binary-oxide phases—In_6WO_{12} and $In_2(WO_4)_3$—were found to be stable over the range 800–1200°C. Heating the binary-oxide phases above 1200°C resulted in the preferential volatilization of WO_3. Rietveld refinement was performed on three structures using X-ray diffraction data from nominally phase-pure In_6WO_{12} at room temperature and from nominally phase-pure $In_2(WO_4)_3$ at 225°C and 310°C. The indium-rich phase, In_6WO_{12}, is rhombohedral, space group $R\bar{3}$ (rhombohedral), with $Z = 1$, $a = 6.22390(4)$ Å, $\alpha = 99.0338(2)^\circ$ [hexagonal axes: $a_H = 9.48298(6)$ Å, $c = 8.94276(6)$ Å, $a_H/c = 0.9430(9)$]. In_6WO_{12} can be viewed as an anion-deficient fluorite structure in which 1/7 of the fluorite anion sites are vacant. Indium tungstate, $In_2(WO_4)_3$, undergoes a monoclinic–orthorhombic transition around 250°C. The high-temperature polymorph is orthorhombic, space group *Pnca*, with $a = 9.7126(5)$ Å, $b = 13.3824(7)$ Å, $c = 9.6141(5)$ Å, and $Z = 4$. The low-temperature polymorph is monoclinic, space group $P2_1/a$, with $a = 16.406(2)$ Å, $b = 9.9663(1)$ Å, $c = 19.099(2)$ Å, $\beta = 125.411(2)^\circ$, and $Z = 8$. The structures of the two $In_2(WO_4)_3$ polymorphs are similar, consisting of a network of corner sharing InO_6 octahedra and WO_4 tetrahedra.
© 2004 Elsevier Inc. All rights reserved.

Keywords: Indium tungsten oxides; Indium tungstate; In_6WO_{12}; $In_2(WO_4)_3$; Tungstates

1. Introduction

Tungsten oxide reacts with M_2O_3 oxides to form a series of mixed-oxide materials with molar ratios (M_2O_3:WO_3) ranging from 3:1 to 2:9. The number of mixed oxides that form in a given system increases with increasing size of the M^{3+} cation. For example, one mixed oxide is reported in the Al_2O_3–WO_3 system [1], whereas five phases—Y_6WO_{12}, $Y_{10}W_2O_{21}$, $Y_{14}W_4O_{33}$, Y_2WO_6, $Y_2(WO_4)_3$—are reported in the Y_2O_3–WO_3 system [2]. Several more are reported for the Nd_2O_3–WO_3 and La_2O_3–WO_3 systems [3,4].

Mixed-oxides in the In_2O_3–WO_3 system have been studied because of their optical and electrical properties. In_6WO_{12} has been investigated as an electrochromic material and as a neutrino detector [5,6]. $In_2(WO_3)_4$ is reported to be a trivalent-cation conductor [7].

Reactions in the In_2O_3–WO_3 system have been studied previously [8], but it was unclear, at the onset of the current study, whether or not the two reported phases—In_6WO_{12} and $In_2(WO_4)_3$—were the only mixed-oxide phases that formed. Moreover, there was limited information regarding the temperature ranges over which the mixed-oxide phases formed, and there were discrepancies in the literature regarding the crystal structures of $In_2(WO_4)_3$. Swanson and Anderson [9] described $In_2(WO_4)_3$ as orthorhombic with unit cell dimensions of $a = 10.72$ Å, $b = 13.04$ Å, and $c = 10.35$ Å whereas Nassau et al. [10] reported unit cell dimensions of $a = 9.3$ Å, $b = 13.3$ Å, and $c = 9.3$ Å. Köhler et al. reported a monoclinic-orthorhombic transformation at 250–260°C and indicated that the low-temperature form is isostructural with $Eu_2(WO_4)_3$ [11]. Sleight et al. reported that the low-temperature form is isostructural with $Fe_2(MoO_4)_3$, crystallizing in $P2_1/a$ with unit cell dimensions of $a = 16.359$ Å, $b = 9.632$ Å, $c = 19.006$ Å, and $\beta = 125.30^\circ$ [12].

*Corresponding author. Fax: +(607)-871-3047.
E-mail address: dedwards@alfred.edu (D.D. Edwards).

0022-4596/$ - see front matter © 2004 Elsevier Inc. All rights reserved.
doi:10.1016/j.jssc.2004.04.015

In this work, X-ray diffraction and differential thermal analysis were used to investigate the subsolidus phase relations in the In_2O_3–WO_3 system at 800–1400°C. Rietveld analysis was conducted on three structures—In_6WO_{12} and the two polymorphs of $In_2(WO_4)_3$—using X-ray powder diffraction data.

2. Experimental procedure

Mixed-oxide samples with various molar ratios were prepared and characterized as summarized in Table 1. Most samples were prepared by solid-state reaction using commercially obtained oxide powders as the starting materials. Weighed portions of In_2O_3 (>99.99% purity, Indium Corporation of America) and WO_3 (>99.99% purity, Aldrich Chemical Co.) were moistened with acetone and ground together in an alumina mortar and pestle. After drying to remove the acetone, the mixed-oxide powders were uniaxially pressed into 1/2″(12.5 mm) diameter pellets using an applied pressure of ~0.1 MPa.

Samples with a molar ratio of In_2O_3:$3WO_3$ were also prepared using a solution method. Appropriate portions of a 1 M aqueous solution of $In(NO_3)_3$ (>99.9% cation purity, Indium Corporation of America) and a 1 M aqueous slurry of H_2WO_4 were mixed in a porcelain crucible, dried, and calcined at 750°C. The resulting powder was ground in an alumina mortar and pestle and uniaxially pressed into 1/2″(12.5 mm) diameter pellets.

The pressed pellets were heated at 800–1400°C inside covered high-purity alumina crucibles. The pellets were either sandwiched between two sacrificial pellets or placed in a powder bed of the same composition to avoid contamination from the crucible and to limit volatilization of the constituent powders. After heating for 2 days, the samples were quenched in air, ground into a powder, and analyzed using X-ray diffraction (XRD). If more than one phase were present, the powders were pressed into pellets, reheated, and reanalyzed until consecutive XRD patterns were identical unless noted otherwise in the discussion. Samples heated at <1200°C lost less than 1% of their initial weight upon heating. Tungsten-containing samples heated at >1200°C exhibited excessive weight loss and could not be equilibrated in the open system used in this study.

Routine phase analysis was conducted with a Phillips XRG 3100 diffractometer (Phillips, Inc., USA) using Cu$K\alpha$ radiation (40 kV, 20 mA). Silicon powder was used as an internal standard for lattice parameter measurements. Diffraction patterns were collected over 10–70° 2θ at a stepped scan rate of 0.04° per step and a count time of 4 s per step. Commercial software (Jade 6.0, Materials Data, Inc., USA) was used to calculate the positions of the reflections with respect to the silicon standard and to determine lattice parameters via the least-squares method.

A sample of nominally phase-pure $In_2(WO_4)_3$ was analyzed using differential thermal analysis (Jupiter STA 449C calorimeter, Netzsch Instruments, Inc.,

Table 1
Visual appearance and phase analysis of In_2O_3–WO_3 samples

Compositions (mol% WO_3)	Reaction temperatures (°C)	Color	Phases identified in X-ray pattern
0	1000, 1200	Yellow	In_2O_3
0	1400	Green	In_2O_3
4, 8, 11, 15, 18	1000	Green	$In_2O_3 + In_6WO_{12}$
25	800, 900	Yellow	$In_2O_3 + In_6WO_{12}$
25	1000, 1100, 1200	White	In_6WO_{12}
25	1200→800[a]	White	In_6WO_{12}
25	1300, 1400	Greenish white	$In_2O_3 + In_6WO_{12}$
36	900	Yellow	$In_6WO_{12} + In_2(WO_4)_3$
36	1000, 1100, 1200	White	$In_6WO_{12} + In_2(WO_4)_3$
50	900, 1000	Yellow	$In_6WO_{12} + In_2(WO_4)_3$
50	1100, 1200	White	$In_6WO_{12} + In_2(WO_4)_3$
67	900	Yellow	$In_6WO_{12} + In_2(WO_4)_3$
67	1000, 1100,1200	White	$In_6WO_{12} + In_2(WO_4)_3$
67	1200→800[a]	White	$In_6WO_{12} + In_2(WO_4)_3$
75	800	Yellow + green	$In_2(WO_4)_3 + WO_3$
75	900	Yellow	$In_2(WO_4)_3$
75	1000, 1100, 1200	White	$In_2(WO_4)_3$
75	1300, 1400	White + gray	$In_2(WO_4)_3 + In_6WO_{12}$
83	1000, 1100, 1200	Green	$In_2(WO_4)_3 + WO_3$
87	1000	Green	$In_2(WO_4)_3 + WO_3$
91	1000, 1100, 1200	Green	$In_2(WO_4)_3 + WO_3$
100	1000, 1100, 1200	Green/gray	WO_3

[a] Samples reacted at 1200°C, then held at 800°C for several days.

USA). The sample was heated at a rate of 5°/min from room temperature to 500°C using nitrogen as a purge gas. Data was collected during heating and cooling.

For Rietveld analysis, X-ray diffraction data was collected for nominally phase-pure powders of In_6WO_{12} and $In_2(WO_4)_3$. The In_6WO_{12} powder was prepared by solid-state reaction at 1200°C and dry quenched. The $In_2(WO_4)_3$ powder was prepared at 800°C from solution-derived powders and dry quenched. Data for the In_6WO_{12} powder were collected at room temperature using a thick-sample mount on a Siemens D500 diffractometer (Bruker AXS GmbH) with Bragg–Brentano geometry using Cu$K\alpha$ radiation (40 kV, 30 mA), 0.3° divergence slits, and a scintillation detector. Diffraction patterns were collected over 2–138° 2θ at a step rate of 0.02° per step, 10 s per step. Data for $In_2(WO_4)_3$ were collected at 225°C and 310°C using a Siemens D500 Parabolic Optic (Huber Diffraktionstechnik GmbH) diffractometer equipped with an Osmic GO13N parabolic multilayer optic on the incident beam side and a custom flat multilayer optic on the diffracted beam side with attached furnace, described elsewhere by Misture [13]. The divergence of the beam is on the order of 0.33°. Using Cu$K\alpha$ radiation (40 kV, 30 mA), high-temperature diffraction patterns for $In_2(WO_4)_3$ were collected over 5–120° 2θ at a rate of 0.02° per step, 15 s per step. The sample was a thin layer of $In_2(WO_4)_3$ powder cast from an acetone slurry onto an alumina plate.

All structure refinements and calculations were performed using the General Structural Analysis System (GSAS) suite of programs [14,15]. The convergence criterion was set at 0.01 for the refinements of In_6WO_{12} and orthorhombic $In_2(WO_4)_3$ and at 0.05 for the refinement of monoclinic of $In_2(WO_4)_3$.

The refinement of In_6WO_{12} was conducted on 5899 data points over the range $20<2\theta<138°$. No significant peaks were noted at 2θ $<20°$, so this region was excluded from the refinement. The refinement was conducted in $R\bar{3}$ with $Z=1$ using the structural parameters reported by Michel and Kahn for single crystal In_6WO_{12} as the initial structural model [16]. Complete occupancy of the four atom sites was assumed. Oxygen thermal parameters were held constant at 0.01 Å^2. Small peaks corresponding to In_2O_3 were noted in the pattern, so a second phase was incorporated into the model using the In_2O_3 atom positions reported by Marezio [17]. The In_2O_3 atoms positions and thermal parameters were held constant; only the lattice parameter and phase fraction were refined. Final refinements indicated that the sample contained 1.2 wt% In_2O_3. The peak profiles were described using a pseudo-Voight function with the Finger–Cox–Jephcoat asymmetry parameter. A five-variable shifted Chebychev function was used to describe the background. Convergence was achieved for a refinement with 29 variables, which included phase fractions, lattice parameters for both phases, In_6WO_{12} atom positions and cation thermal parameters, background parameters, and some profile and diffractometer parameters. The residual statistics are as follows: wR_p (total pattern) = 9.74%, R_p (total pattern) = 7.32%, wR_p (background removed) = 8.29% and R_p (background removed) = 6.62%, $R(F^2) = 5.08\%$, and $\chi^2 = 2.091$. Comparison of the observed and calculated intensities of different classes of reflections showed some evidence for [111] preferred orientation. Additional refinements including the March–Dollase function resulted in an orientation parameter of $R_o \sim 0.98$ (compared to $R_o = 1.0$ for a sample without preferred orientation) and a negative thermal parameter for one cation, thus preferred orientation effects are not included in the reported refinement.

For the high-temperature (orthorhombic) phase of $In_2(WO_4)_3$, the refinement was conducted using 5600 data points collected at 310°C. The refinement was conducted in *Pnca* with $Z = 4$ using lattice parameters determined by least-squares analysis and atom positions reported for $Sc_2(WO_4)_3$ [18] as the initial structural parameters. Cation and anion positions were refined assuming complete occupancy of all nine sites. Cation thermal parameters were refined, but oxygen thermal parameters were held at 0.01 Å^2. Indium oxide was included as a secondary phase in the refinement. The atom positions and thermal parameters for In_2O_3 were held constant using the values reported by Marezio [17]. Final refinement indicated 2.2 wt% In_2O_3 in the sample. The background was modeled as 5-variable shifted-Chebychev function, and peak profiles were modeled using the pseudo-Voight function. There was no evidence of preferred orientation. Convergence was achieved for a refinement of 45 variables, which included phase fractions, lattice parameters for $In_2(WO_4)_3$, atom positions and cation thermal parameters for $In_2(WO_4)_3$, background parameters, and some profile and diffractometer parameters. The final refinement resulted in the following residual statistics: wR_p (total pattern) = 12.12%, and R_p (total pattern) = 9.28%, wR_p (background removed) = 11.17% and R_p (background removed) = 8.85%, $R(F^2) = 8.84\%$, and $\chi^2 = 1.906$.

For the low-temperature (monoclinic) phase of $In_2(WO_4)_3$, the refinement was conducted using 5600 data points collected at 225°C. The refinement was conducted in $P\ 2_1/a$ with $Z = 8$ using the lattice constants reported by Sleight and Brixner [12] as the initial parameters. Initial atom coordinates were taken as those reported by Chen for $Fe_2(MoO_4)_3$ with In replacing Fe and W replacing Mo [19]. Full occupancy of all 34 sites was assumed. Trial refinements involving oxygen positions and thermal parameters led to unreasonable bond lengths and bond angles, so the oxygen positions were held constant at the values

reported by Chen and oxygen thermal parameters were held constant at 0.01 Å^2. A 5-variable shifted-Chebychev function was used described the background. Peak profiles were described using the pseudo-Voight function. Indium oxide was included as a secondary phase. Final refinements indicated 1.0 wt% In_2O_3 in the final sample. Convergence was achieved for a refinement of 60 variables which included phase fractions of both phases and lattice parameters of both phases, atom positions and cation thermal parameters for $In_2(WO_4)_3$, background parameters, some profile parameters, and some diffractometer parameters. The residual statistics of the final refinement were as follows: wR_p (total pattern) = 12.42%, and R_p (total pattern) = 9.45%, wR_p (background removed) = 11.52% and R_p (background removed) = 9.02%, $R(F^2) = 7.29\%$, and $\chi^2 = 1.936$.

3. Results and discussion

3.1. Subsolidus phase relations in In_2O_3–WO_3 system

Fig. 1 shows the X-ray diffraction patterns of samples prepared at 1000°C. Based on comparisons to powder diffraction files (International Centre for Diffraction Data, Newtown Square, PA), four distinct phases are evident, including In_2O_3, In_6WO_{12}, $In_2(WO_4)_3$, and WO_3.

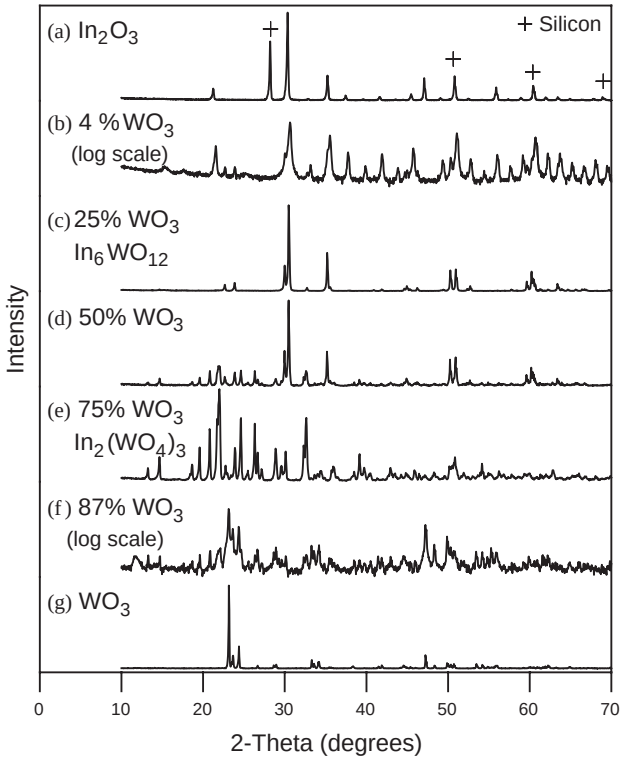

Fig. 1. As-collected room-temperature X-ray diffraction patterns of mixed oxide samples prepared at 1000°C. Four distinct phases are evident, including In_2O_3, In_6WO_{12}, $In_2(WO_4)_3$, and WO_3. The intensity for samples prepared with 4 and 87% WO_3 is presented on a log scale to enable identification of minor phases; the intensity for all other patterns is plotted on a linear scale.

Powders prepared with 25 mol% WO_3 reacted to form nominally phase-pure In_6WO_{12} when heated at 1000°C and 1200°C. The resulting pellets were white and the corresponding XRD patterns were well matched with powder diffraction file for In_6WO_{12} (PDF #74-1410). Samples prepared at 800°C and 900°C were yellow, suggesting the presence of unreacted In_2O_3, which was confirmed by X-ray diffraction analysis. Nevertheless, samples initially reacted at 1200°C and then annealed at 800°C showed no evidence of disassociation, which suggests that In_6WO_{12} is stable at 800°C. Samples heated at 1300°C and 1400°C exhibited significant weight loss. The corresponding X-ray diffraction patterns showed evidence of In_2O_3 in addition to In_6WO_{12}, suggesting the preferential volatilization of WO_3.

Sample prepared with 75 mol% WO_3 at 1000°C and 1200°C were white, and their X-ray diffraction patterns were well matched to the powder diffraction file for $In_2(WO_4)_3$ (PDF # 49-0337), which reports reflections over 10–34° 2-Θ Cu$K\alpha$. The sample prepared at 800°C was a multiphase mixture, containing WO_3 in addition to $In_2(WO_4)_3$. Nevertheless, samples of $In_2(WO_4)_3$ initially reacted at 1200°C and then annealed at 800°C showed no evidence of disassociation, suggesting that $In_2(WO_4)_3$ is stable at 800°C. This assertion was also confirmed by the preparation of nominally phase-pure $In_2(WO_4)_3$ at 800°C from solution-derived powders. Samples prepared at 1400°C were covered with a layer of needle-like gray material, which was identified as In_6WO_{12} by X-ray diffraction. Thus, the excessive weight loss of the samples prepared at 1300°C and 1400°C was attributed to the preferential loss of WO_3.

Fig. 2 summarizes the subsolidus phase relationships in the In_2O_3–WO_3 system. With the exception of In_2O_3, no attempts were made to determine whether or not the phases formed limited solid solutions, so all phases are shown as line compounds. In the case of In_2O_3, mixed-oxide samples prepared with 4% WO_3 contained In_6WO_{12} as well as In_2O_3 suggesting that the solubility limit of WO_3 in In_2O_3 is less than 4 mol%. Since oxygen content was not measured in this study, all phases are shown to be complete oxidized. (Under more reducing conditions, phases expressed as WO_{3-x}, $x<1$ and as In_xWO_3, $x<0.3$ are known to form [20,21].) Phase relationships above 1200°C are not presented since equilibrium could not be achieved in the open-air system used in this study.

3.2. Crystal structure of In_6WO_{12} and its relationship to In_2O_3

Fig. 3 shows the observed, calculated, and difference profiles for the refinement of In_6WO_{12}. Table 2

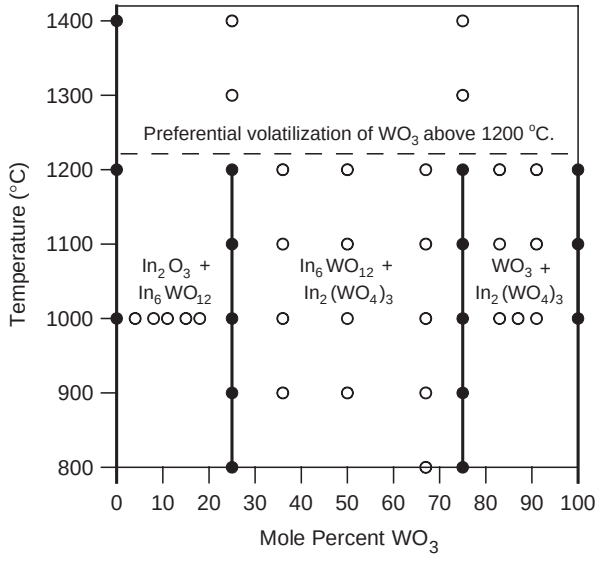

Fig. 2. Formation diagram for the In_2O_3–WO_3 system at 800–1400°C. Filled circles indicate nominally phase-pure materials. Open circles indicate biphasic samples. Subsolidus phase relationships are shown for temperature $\leqslant$1200°C. Above 1200°C, equilibrium conditions could not be achieved in the open-air system due to preferential volatilization of WO_3.

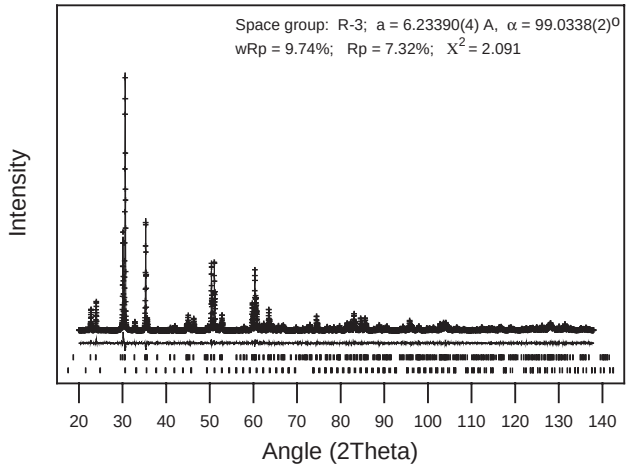

Fig. 3. Observed, calculated, and difference X-ray powder diffraction patterns of In_6WO_{12} at room temperature. The top set of tick marks corresponds to In_6WO_{12}; the bottom set corresponds to In_2O_3.

summarizes the structural parameters, and Table 3 summarizes selected interatomic distances and angles. The refined lattice parameters for the polycrystalline specimen used in this study (rhombohedral: $a_R = 6.23390(4)$ Å, $\alpha = 99.0338(2)^\circ$ or hexagonal: $a_H = 9.48298(6)$ Å, $c = 8.94276(6)$ Å, $a_H/c = 0.9430(9)$) are in reasonably good agreement with those reported for a single-crystal specimen by Michel and Kahn ($a_R = 6.2277(9)$ Å, $\alpha = 99.01(1)^\circ$, or hexagonal: $a_H = 9.472(2)$ Å, $c = 8.939(2)$ Å, $a_H/c = 0.9438(2)$) [16]. The cation positions and cation–anion bond lengths also in good agreement with those reported previously by Michel and Kahn [16].

The structure of In_6WO_{12}, like that of In_2O_3, can be described as an anion-deficient fluorite structure. In the case of In_6WO_{12}, one-seventh of the fluorite anion sites are vacant. Ordering of the structural anion vacancies along the $\langle 111 \rangle$ direction of the parent fluorite structure leads to rhombohedral symmetry and the occurrence of WO_6 and InO_7 polyhedra. In the case of In_2O_3, one-fourth of the fluorite anion sites are vacant, resulting in two distinct InO_6 octahedra—one with structural vacancies located along the body diagonal of the fluorite cube and one with structural vacancies located along the face diagonal of the fluorite cube [17]. The body-diagonal vacancy arrangement in In_2O_3 results in a nearly regular InO_6 octahedra similar to the WO_6 octahedra found in In_6WO_{12}.

Despite the availability of a favorable cation environment and a large fraction of structural anion vacancies in In_2O_3 structure, a significant amount of WO_3 is not incorporated to form a random solid solution. Instead, there is a preference for cation ordering, which results in the formation mixed-phase samples of In_2O_3 and In_6WO_{12} in samples with WO_3 concentrations as low as 4 mol percent.

3.3. Crystal structures of $In_2(WO_4)_3$

The $In_2(WO_4)_3$ investigated in this study exhibited a reversible phase transition at 242–250°C as illustrated in Fig. 4. Koehler et al. [11] and Sleight and Brixner [12]

Table 2
Structural parameters for In_6WO_{12} (space group $R\bar{3}$; $a = 6.23390(4)$ Å, 99.0338(2)°)

Atom	Position	x	y	z	U
W	1*a*	0.0	0.0	0.0	0.0003(4)
In	6*f*	0.1395 (1)	0.3224 (1)	0.6046 (1)	0.0028 (2)
O_1	6*f*	−0.048 (1)	0.090 (2)	0.290 (1)	0.01[a]
O_2	6*f*	0.413 (1)	0.589 (1)	0.836 (1)	0.01[a]

Total pattern: $wR_p = 0.0974$; $R_p = 0.0732$; $\chi^2 = 2.091$
Background removed: $wR_p = 0.0829$; $R_p = 0.0662$

[a] Isotropic thermal factors held constant during refinement.

Table 3
Selected interatomic distances (Å) and bond angles (°) in In_6WO_{12}

Bond lengths (Å)		Bond angles (°)	
WO_6			
W–O_1 (× 6)	1.892(7)	O_1–W–O_1 (× 6)	95.1(3)
		O_1–W–O_1 (× 6)	84.9(3)
InO_7			
In–O_1	2.272(2)	O_1–In–O_1	125.2(3)
In–O_1	2.269(8)	O_1–In–O_2	80.0(3
In–O_1	2.750(8)	O_1–In–O_2	87.8(3)
In–O_2	2.309(6)	O_1–In–O_2	89.6(3)
In–O_2	2.052(7)	O_1–In–O_2	74.9(2)
In–O_2	2.195(8)	O_1–In–O_2	81.7(3)
In–O_2	2.094(7)	O_1–In–O_2	99.6(3)
		O_2–In–O_2	78.4(3)
		O_2–In–O_2	80.4(3)
		O_2–In–O_2	77.2(3)

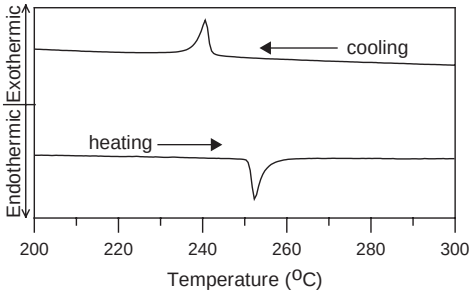

Fig. 4. Differential thermal analysis curve for $In_2(WO_4)_3$ in air.

previously reported an orthorhombic–monoclinic phase transition at 250–260°C and 252°C, respectively.

Fig. 5 shows the observed, calculated, and difference profiles for the refinement of $In_2(WO_4)_3$ at 310°C. The refined lattice parameters are in closer agreement with those reported by Nassau et al. [10] for powder samples than to those reported by Swanson and Anderson [9] for single crystal data. The refined atom coordinates, summarized in Table 4, are similar to those reported by Evans et al. for $Sc_2(WO_4)_3$ [18].

Select interatomic distances and bond angles for $In_2(WO_4)_3$ at 310°C are presented in Tables 5 and 6, respectively. The In–O distances range from 2.03 to 2.23 Å, which are comparable to the In–O distances reported by Marezio [17] in In_2O_3 (2.13–2.23 Å) and the Sc–O distances reported by Evans et al. [18] for $Sc_2(WO_4)_3$ (2.079–2.109 Å). The InO_6 octahedra appear to be somewhat distorted with O–In–O angles ranging from 80.0° to 98.3°. The W–O distances (1.66–1.89 Å) are comparable to those reported for WO_3 (1.72–2.16 Å) and for $Sc_2(WO_4)_3$ (1.74–1.765 Å) [18,22]. The WO_4 tetrahedra are somewhat distorted as well with O–W–O bond angles, ranging from 99.9 to 124°.

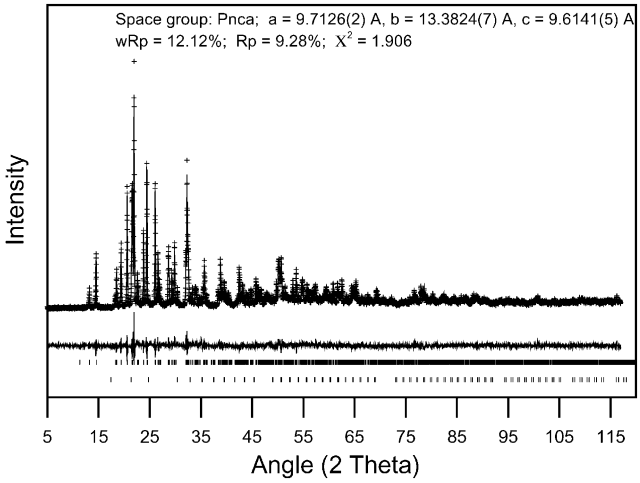

Fig. 5. Observed, calculated, and difference X-ray powder diffraction patterns of the orthorhombic form of $In_2(WO_4)_3$ at 310°C (583 K). The top set of tick marks corresponds to $In_2(WO_4)_3$; the bottom set corresponds to In_2O_3.

Table 4
Structural parameters of $In_2(WO_4)_3$ at 310°C (583 K) (space group *Pnca*; $a = 9.7126(5)$ Å, $b = 13.3824(7)$ Å, and $c = 9.6141(5)$ Å)

Atom	Position	x	y	z	U
In	8*d*	0.4673(3)	0.3819(2)	0.2494(4)	0.023(2)
W_1	4*c*	0.2500	0.0000	0.4716(4)	0.027(2)
W_2	8*d*	0.1162(2)	0.3551(2)	0.3942(3)	0.027(2)
O_1	8*d*	0.106(2)	0.151(2)	0.091(2)	0.01[a]
O_2	8*d*	0.141(2)	0.065(2)	0.353(3)	0.01[a]
O_3	8*d*	−0.022(2)	0.272(2)	0.318(2)	0.01[a]
O_4	8*d*	0.331(2)	0.391(2)	0.064(2)	0.01[a]
O_5	8*d*	0.071(2)	0.464(2)	0.325(3)	0.01[a]
O_6	8*d*	0.301(2)	0.330(2)	0.354(2)	0.01[a]

Total pattern: $wR_p = 0.1212$; $R_p = 0.0928$; $\chi^2 = 1.906$
Background removed: $wR_p = 0.1117$; $R_p = 0.0885$

[a] Isotropic thermal factors held constant during refinement.

Table 5
Select interatomic distances (Å) in $In_2(WO_4)_3$ at 310°C (583 K)

InO_6 octahedra		WO_4 tetrahedra	
In_1–O_1	2.09(2)	W_1–O_2 (× 2)	1.78 (2)
In_1–O_2	2.08(2)	W_1–O_4 (× 2)	1.88 (2)
In_1–O_3	2.16(2)		
In_1–O_4	2.23 (2)		
In_1–O_5	2.22 (2)	W_2–O_1	1.89(2)
In_1–O_6	2.03 (2)	W_2–O_3	1.89(2)
		W_2–O_5	1.66(2)
		W_2–O_6	1.87(2)

Fig. 6 shows the observed, calculated, and difference profiles for the refinement of $In_2(WO_4)_3$ at 225°C. The corresponding atomic coordinates are presented in Table 7. The refined lattice parameters of $a = 16.4044$

Table 6
Select bond angles (degrees) in $In_2(WO_4)_3$ at 310°C (583 K)

InO_6 octahedra		WO_4 tetrahedra	
O_1–In_1–O_2	83.9(9)	O_2–W_1–O_2	100 (2)
O_1–In_1–O_3	89.5(9)	O_2–W_1–O_4 (× 2)	115.5 (9)
O_1–In_1–O_5	93.6(8)	O_2–W_1–O_4 (× 2)	99.9 (9)
O_1–In_1–O_6	94.4(9)	O_4–W_1–O_4	124 (1)
O_2–In_1–O_3	98.3(8)		
O_2–In_1–O_4	94.8(9)		
O_2–In_1–O_5	88.4(8)		
O_3–In_1–O_4	80.9(8)	O_1–W_2–O_3	109(1)
O_3–In_1–O_6	82.0(9)	O_1–W_2–O_5	115(1)
O_4–In_1–O_5	96.2(8)	O_1–W_2–O_6	104(1)
O_4–In_1–O_6	86.9(8)	O_3–W_2–O_5	100(1)
O_5–In_1–O_6	91.4(9)	O_3–W_2–O_6	120(1)
		O_5–W_2–O_6	109(1)

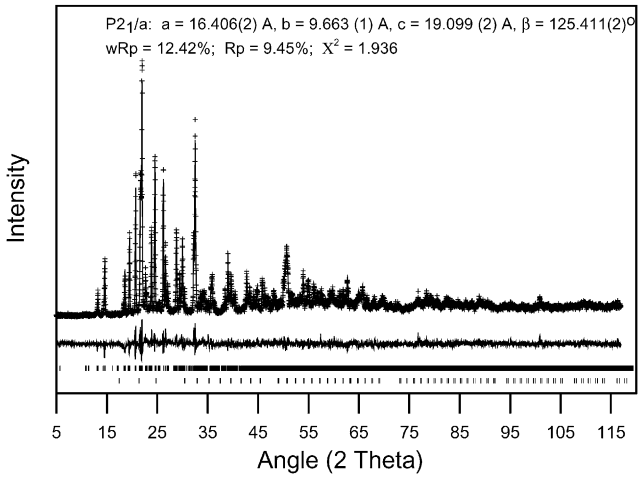

Fig. 6. Observed, calculated, and difference X-ray powder diffraction patterns of the monoclinic form of $In_2(WO_4)_3$ at 225°C (498 K). The top set of tick marks corresponds to $In_2(WO_4)_3$; the bottom set corresponds to In_2O_3.

(4) Å, $b = 9.6616(2)$ Å, $c = 19.0964(5)$ Å, and $\beta = 125.408(2)^\circ$ are comparable to those reported by Sleight and Brixner [12]. The refined cation coordinates are similar to those reported for the $Fe_2(MoO_4)_3$ [19].

Since the oxygen positions could not be refined for the monoclinic structure, there is considerable uncertainty regarding the oxygen positions reported in Table 7. Notwithstanding, calculated M–O bond lengths are reported in Table 8 to demonstrate that the refined cation positions did not lead to unreasonable interatomic distances.

As illustrated in Fig. 7, the two polymorphs of $In_2(WO_4)_3$ are closely related. Both structures can be described as a corner-sharing network of WO_4 tetrahedra and InO_6 octahedra with each WO_4 tetrahedra sharing its vertices with four InO_6 octahedra and each InO_6 octahedra sharing its vertices with six WO_4 tetrahedra. (The InO_6 octahedra are not explicitly shown in Fig. 7). The lattice vectors of the two cells

Table 7
Structural parameters of $In_2(WO_4)_3$ at 225°C (498 K) (space group $P2_1/a$; $a = 16.406(2)$ Å, $b = 9.663(1)$ Å, $c = 19.099(2)$ Å, and $\beta = 125.411(2)^\circ$

Atom	Position	x	y	z	U
W_1	4e	−0.008(1)	0.249(2)	0.4856(7)	0.033(4)
W_2	4e	0.3562(9)	0.111(2)	0.1304(7)	0.028(4)
W_3	4e	0.1401(8)	0.113(1)	0.2558(6)	0.025(4)
W_4	4e	0.149(1)	0.615(2)	0.3826(7)	0.047(5)
W_5	4e	0.3516(8)	0.630(1)	0.2169(7)	0.029(4)
W_6	4e	−0.002(1)	0.749(2)	0.0184(7)	0.031(3)
In_1	4e	0.381(2)	0.964(2)	0.317(1)	0.024(6)
In_2	4e	0.372(1)	0.457(2)	0.051(1)	0.037(6)
In_3	4e	0.120(2)	0.473(3)	0.187(1)	0.023(5)
In_4	4e	0.107(1)	0.984(2)	0.419(1)	0.026(6)
O_1[a]	4e	0.5817	0.3872	−0.0001	0.01
O_2[a]	4e	0.9882	0.4075	0.1715	0.01
O_3[a]	4e	0.8280	0.1937	0.0949	0.01
O_4[a]	4e	0.7744	0.4974	0.0544	0.01
O_5[a]	4e	0.5225	0.4253	0.1443	0.01
O_6[a]	4e	0.7321	0.5194	0.2728	0.01
O_7[a]	4e	0.4204	0.1099	0.4139	0.01
O_8[a]	4e	0.1843	0.2854	0.2464	0.01
O_9[a]	4e	0.5482	0.3536	0.4437	0.01
O_{10}[a]	4e	0.3877	0.3088	0.9753	0.01
O_{11}[a]	4e	0.0644	0.3818	0.0674	0.01
O_{12}[a]	4e	0.4115	0.3627	0.5010	0.01
O_{13}[a]	4e	0.8575	0.3829	0.2325	0.01
O_{14}[a]	4e	0.2484	0.0396	0.5128	0.01
O_{15}[a]	4e	0.1164	0.1065	0.3324	0.01
O_{16}[a]	4e	0.5327	0.9432	0.3626	0.01
O_{17}[a]	4e	0.7422	0.9597	0.1926	0.01
O_{18}[a]	4e	0.6654	0.9378	0.3007	0.01
O_{19}[a]	4e	0.9619	0.9339	0.3116	0.01
O_{20}[a]	4e	0.0945	0.3111	0.5939	0.01
O_{21}[a]	4e	0.1568	0.8062	0.3913	0.01
O_{22}[a]	4e	0.0451	0.6577	0.1210	0.01
O_{23}[a]	4e	0.3629	0.6027	0.1228	0.01
O_{24}[a]	4e	0.3438	0.8171	0.2257	0.01

Total pattern: $wR_p = 0.1242$; $R_p = 0.0945$; $\chi^2 = 1.936$
Background removed: $wR_p = 0.1152$; $R_p = 0.0902$

[a] Atomic coordinates and isothermal temperature factors held constant during refinement.

are approximately related as follows:

$$\begin{pmatrix} a_m \\ b_m \\ c_m \end{pmatrix} = \begin{pmatrix} 0 & 1 & -1 \\ 1 & 0 & 0 \\ 0 & 0 & 2 \end{pmatrix} \begin{pmatrix} a_o \\ b_o \\ c_o \end{pmatrix}.$$

Both forms of $In_2(WO_4)_3$ can be viewed as layered structures with planes of In^{3+} cations—a feature that is often cited as the reason for the relatively high ionic conductivity in structurally related tungstates and molybdates, such as $Sc(WO_4)_3$ and $Sc(MO_4)_3$.[7] In the orthorhombic form of $In_2(WO_4)_3$, the In sites lie within ±0.006 Å of planes located perpendicular to the c-axis at $z = 0.25$ and $z = 0.75$. In the monoclinic structure, the indium sites are less coplanar, lying within ±0.2 Å of planes that are perpendicular to the c-axis.

Table 8
Select interatomic distances (Å) in $In_2(WO_4)_3$ at 225°C(498 K)

InO_6 octahedra		WO_4 tetrahedra	
In_1–O_6	2.07(2)	W_1–O_7	1.80(2)
In_1–O_7	2.10(2)	W_1–O_9	1.82(1)
In_1–O_{13}	2.06(2)	W_1–O_{12}	1.86(1)
In_1–O_{16}	2.12(2)	W_1–O_{20}	1.85(1)
In_1–O_{20}	2.11(2)		
In_1–O_{24}	2.05(2)	W_2–O_2	1.84(1)
		W_2–O_3	1.97(1)
In_2–O_1	2.15(2)	W_2–O_4	1.66(1)
In_2–O_3	2.01(2)	W_2–O_{13}	1.94(1)
In_2–O_4	2.10(2)		
In_2–O_5	2.07(2)	W3–O_5	1.91(1)
In_2–O_{10}	2.16(2)	W3–O_6	1.86(1)
In_2–O_{23}	2.03(2)	W3–O_8	1.87(1)
		W3–O_{15}	1.72(1)
In_3–O_2	2.10(2)		
In_3–O_8	2.08(2)	W_4–O_{14}	1.86(1)
In_3–O_{11}	2.10(2)	W_4–O_{16}	1.80(2)
In_3–O_{17}	2.06(2)	W_4–O_{18}	1.81(1)
In_3–O_{18}	2.03(2)	W_4–O_{21}	1.86(2)
In_3–O_{22}	2.11(2)		
		W_5–O_{17}	1.79(1)
In_4–O_9	2.04(2)	W_5–O_{19}	1.77(1)
In_4–O_{12}	2.09(2)	W_5–O_{23}	1.93(1)
In_4–O_{14}	2.01(2)	W_5–O_{24}	1.83(1)
In_4–O_{15}	2.11 (2)		
In_4–O_{19}	2.11(2)	W_6–O_1	1.76(2)
In_4–O_{21}	2.10 (2)	W_6–O_{10}	1.90(1)
		W_6–O_{11}	1.84(2)
		W_6–O_{22}	1.86(1)

4. Conclusions

Subsolidus phase equilibria in the In_2O_3–WO_3 system in air at 800–1400°C were investigated using X-ray diffraction and differential thermal analysis. Both binary oxides in the system—In_6WO_{12} and $In_2(WO_4)_3$ are stable at 800–1200°C. At 1200°C and above, both binary oxide phases exhibit preferential loss of WO_3. The structural parameters obtained from the Rietveld refinement of In_6WO_{12} using powder X-ray diffraction data collected at room temperature was in good agreement with previous reports involving single crystal material. Crystallizing in $R\bar{3}$, In_6WO_{12} has a fluorite-related structure in which 1/7 of the anion sites are vacant. Differential thermal analysis of $In_2(WO_4)_3$ confirmed an orthorhombic–monoclinic phase transition near 250°C. Rietveld analysis indicated that the high-temperature (orthorhombic) form, which crystallizes in *Pnca*, is isostructural with $Sc_2(WO_4)_3$ and that the low-temperature (monoclinic form), which crystallizes in $P2_1/a$, is isostructural with $Fe_2(MoO_4)_3$. The two polymorphs of $In_2(WO_3)_4$ have closely related structures, both of which can be described as having a network of corner-sharing InO_6 octahedra and WO_4 tetrahedra.

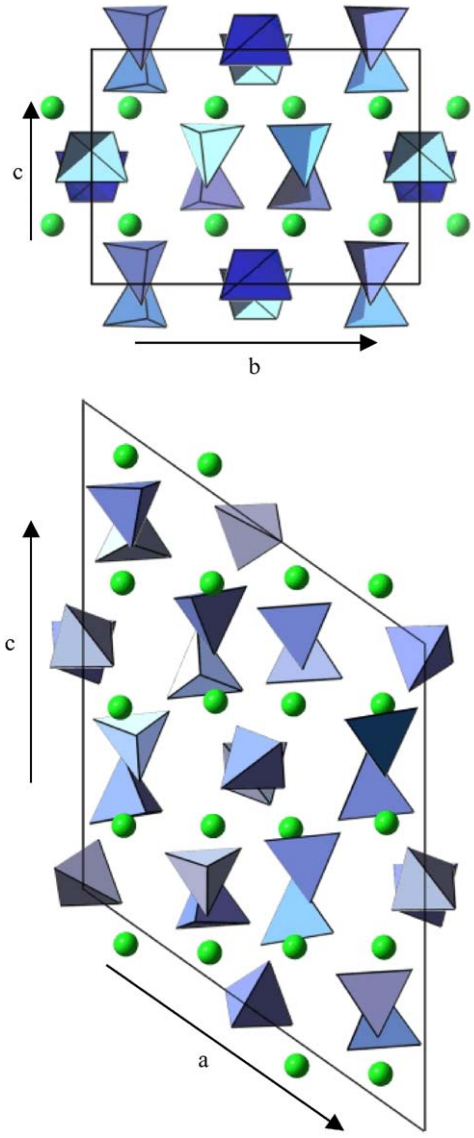

Fig. 7. The orthorhombic and monoclinic structures of $In_2(WO_4)_3$. The WO_4 polyhedra are in blue; the indium ions are shown in green.

Acknowledgments

The authors thank Mick Dolan and Slawomir Zdzieszynski for assistance with the high temperature X-ray diffraction measurements and Scott Misture for constructive discussions. Funding for A.P. Richard was provided by the New York State College of Ceramics (SUNY) and by the Alcoa Foundation.

References

[1] J.L. Waring, J. Am. Ceram. Soc. 48 (9) (1965) 493–494.
[2] K. Kuribayashi, M. Yoshimura, T. Ohta, T. Sata, J. Am. Ceram. Soc. 64 (11–12) (1980) 644–647.

[3] E.Ya. Rode, V.N. Karpov, Inorg. Mater. 2 (4) (1960) 587–590.
[4] M.M. Ivanova, G.M. Balagina, E.Ya. Rode, Inorg. Mater. 6 (5) (1970) 803–805.
[5] T. Gaewdang, J.P. Chaminade, A. Garcia, C. Fouassier, M. Pouchard, P. Hagenmuller, Mater. Lett. 18 (1993) 64–68.
[6] W.S. Dabney, N.E. Antolino, B.S. Luisi, A.P. Richard, D.D. Edwards, Thin Solid Films 411 (2002) 192–197.
[7] G. Adachi, N. Imanaka, S. Tamura, Solid State Ion. (2001) 534–539.
[8] V.K. Trunov, L.M. Kovba, Moscow Univ. Chem. Bull. 22 (1) (1967) 91–93.
[9] A.B. Swanson, J.S. Anderson, Mater. Res. Bull. 3 (1968) 149–152.
[10] K. Nassau, H.J. Levinstein, G.M. Loiacono, J. Phys. Chem. Solids 26 (1965) 1805–1816.
[11] J. Kohler, N. Imanaka, G. Adachi, Z. Anorg. Allg. Chem. 625 (1999) 1890–1896.
[12] A.W. Sleight, L.H. Brixner, J. Solid State Chem. 7 (1973) 172–174.
[13] S.T. Misture, Meas. Sci. Technol. 14 (7) (2003) 1091–1098.
[14] A.C. Larson, R.B. Von Dreele, Los Alamos National Laboratory Report LAUR 86-748, 2000.
[15] B.H. Toby, J. Appl. Crystallogr. 34 (2001) 210–213.
[16] D. Michel, A. Kahn, Acta. Crystallogr. Sect B: Crystallogr. Cryst. Chem. 38 (1982) 1437–1441.
[17] M. Marezio, Acta Crystallogr. 20 (1966) 723–728.
[18] J.S.O. Evans, T.A. Mary, A.W. Sleight, J. Solid State Chem. 137 (1998) 148–160.
[19] H. Chen, Mater. Res. Bull. 14 (1979) 1583–1590.
[20] H.A. Wriedt, Bull. Alloy Phase Diagrams 10 (4) (1989) 368–384.
[21] T. Ekstrøm, M. Parmentier, K.A. Watts, R.J.D. Tilley, J. Solid State Chem. 4 (1984) 365–377.
[22] B.O. Loopstra, P. Boldrini, Acta Crystallogr. 21 (1966) 158–162.